EPJ Web of Conferences **185**, 05012 (2018) https://doi.org/10.1051/epjconf/201818505012
MISM 2017

Ternary phase diagram of Ni-Mn-Ga: insights from *ab initio* calculations

Yulia Sokolovskaya[1], *Mikhail* Zagrebin[1,2,⋆], *Vasiliy* Buchelnikov[1], and *Alexey* Zayak[3]

[1] *Chelyabinsk State University, 454001 Chelyabinsk, Russia*
[2] *National Reserach South Ural State University, 454080 Chelyabinsk, Russia*
[3] *Bowling Green State University, OH-43403 Bowling Green, USA*

Abstract. In this work we perform a wide-range systematic study of the family off-stoichiometric Ni-Mn-Ga alloys by using the supercell approach in the framework of density functional theory. Our goal is to explore the compositional variations of the structural stability and magnetic properties of Ni-Mn-Ga compositions. As a result equilibrium lattice parameters, bulk moduli, total magnetic moments, and formation energies of a wide range of Heusler alloys have been mapped on compositional ternary diagrams.

1 Introduction

Heusler alloys represent a large family of ternary metallic compounds that became known at first as magnetic shape-memory effect materials. Sometime later, more Heusler alloys became known as half-metals, promising for realizing spintronic technologies. Another subgroup of Heusler alloys is explored with respect to the magnetocaloric effect (magnetic refrigeration). A large number of Heusler family members and the richness of properties exhibited by them make this class of materials well suitable for emerging materials dependent technologies [1–3]. At present, Ni-Mn-Ga Heusler systems are the most studied among many ferromagnetic (FM) shape memory alloys. Such high interest is related to the unique properties exhibited by the prototypical stoichiometric shape-memory compound Ni_2MnGa [1–3]. A variety of different off-stoichiometric Ni-Mn-Ga compositions, which have been synthesized and characterized in the past twenty years are mapped on the ternary diagram. However, the most popular compositions are localized in the middle part of a ternary diagram, close to the stoichiometric system. The majority of well-studied compounds belong to the families of $Ni_{2+x}Mn_{1-x}Ga$ ($x = 0.0-0.39$) and $Ni_2Mn_{1+x}Ga_{1-x}$ ($x = 0.0 - 0.40$), showing a strong coupling between the magnetic and structural subsystems [1, 4].

In the previous studies, we presented ternary compositional phase diagrams that showed the variability of several major physical properties as a function of the chemical composition of Ni-Mn-Ga [5–7]. Those diagrams are compositional maps that show the most stable alloy compositions, or compositions that exhibit the largest magnetic moment, or those compositions that represent the hardest crystal structure. That was a proof-of-principle step, which showed that even compositions of Heusler alloys, which are far from the stoichiometric one, could have significant potential for exploring. However, those calculations had been done with the KKR-CPA method, which is great for studying random compounds, however, may lack the detailed chemical accuracy of the local chemical bonding, due to the mean-field approximation used in this method.

Our current study is reproducing of the ternary diagrams described above, but using the more accurate supercell approach, which takes into account local chemical effects without the mean-field approximation.

In this work, we perform a wide-range systematic study of the off-stoichiometric Ni-Mn-Ga alloys using the supercell approach in the framework of density functional theory.

2 *Ab initio* computational details

All calculations were performed using the density functional theory as part of VASP (Vienna *ab initio* simulation program) [8, 9]. This code is based on the projector augmented wave (PAW) method. The generalized gradient approximation (GGA) according to the Perdew-Burke-Ernzerhof (PBE) parametrization [10] was used to take into account the exchange correlation effects. Ground state calculations were performed with the help of the supercell approach with 16-atom supercell. With respect to the pseudopotentials in VASP calculations we used the next electronic configurations: Ni($3p^6 3d^8 4s^2$), Mn($3p^6 3d^6 4s^1$), Ga($3d^{10} 4s^2 4p^1$), respectively. The kinetic energy cut-off was 400 eV and the kinetic energy cut-off for the augmentation charges was 800 eV. The k-points in the Brillouin zone for self-consistent field cycles were generated with 8^3 meshes for lattice relaxation calculations. To estimate the optimized lattice constants for all alloys under study, we fitted the dependences of total energy on a cell volume according to the Birch-Murnagahan equation of state. To investigate the phase stability of the

⋆ e-mail: miczag@mail.ru

Ni-Mn-Ga compounds, we calculate their formation energies for the cubic phase. It should be noted that the formation energy is defined as a difference between the total energy of the alloy and the concentration weighted average of the pure atomic species, as follows:

$$E_{form} = E_{tot} - \left(x \times E^{\mathrm{Ni}} + y \times E^{\mathrm{Mn}} + z \times E^{\mathrm{Ga}}\right), \qquad (1)$$

where, E_{tot} is the total energy of alloy, x, y, z and $E^{\mathrm{Ni(Mn,Ga)}}$ are the concentrations and pure element total energy of Ni, Mn, Ga atoms, respectively. The negative value of formation energy indicates the phase stability.

In this study, we considered 105 compositions presented in Fig. 1. Three of them are stoichiometric (Ni_2MnGa, Mn_2NiGa, and Ga_2MnNi).

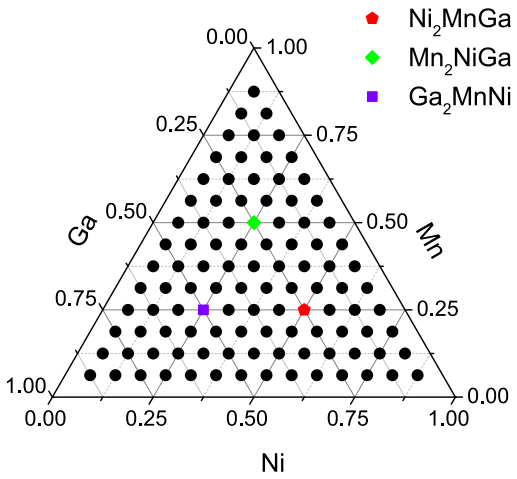

Figure 1. Ternary phase diagram of Ni-Mn-Ga alloys. Symbols indicate the compositions for which the calculations were performed. Color symbols indicate stoichiometric compositions: Ni_2MnGa, Mn_2NiGa, and Ga_2MnNi.

We used four types of crystal lattices to create off-stoichiometric compositions. The first one is the #225 ($Fm\bar{3}m$) symmetry group. In this case, for all compositions we fixed Ni, Mn, and Ga atoms at 8*c*, 4*b*, and 4*a* Wyckoff positions, respectively. The second one is the same as #225 ($Fm\bar{3}m$) symmetry group, and we used this type in a case there are no less than 8 Mn atoms in the supercell. In this case the Mn atoms are placed in 8*c* Wyckoff positions, Ni and Ga atoms in 4*a*, and 4*b* positions, respectively. This type was denoted as #225'. In the third type (which we denoted as #225") Ga atoms are placed in 8*c* Wyckoff positions, Mn and Ni atoms in 4*a*, and 4*b* positions, respectively. This case is used for compounds containing 8 and more Ga atoms. The last crystal structure is of #216 ($F\bar{4}3m$) symmetry group. In this case Mn atoms are placed in 4*c* and 4*a* positions, Ga and Ni atoms in 4*b*, and 4*d* positions, respectively. Positions of Ni, Mn and Ga atoms for all considered types of crystal lattices are listed in Table 1.

As known, an antiferromagnetic (AFM) interactions between Mn atoms located in different sublattices are realized in nonstoichiometric alloys Ni-Mn-Ga. It is necessary to consider the different magnetic configurations of the Mn atoms. For compositions with the Ni and Ga excess, we considered three magnetic configurations refereed as FM (spins of Mn located at the Ni, Mn, and Ga sites are parallel) and two ferrimagnetic (FIM) ones: FIM-1 and FIM-2. For compositions with Mn excess the one FM and seven FIM magnetic configurations were considered. Sign of Mn atoms in different sublattices are listed in Table 2.

Table 1. Positions of the Ni, Mn and Ga atoms in the different crystal structures used in our calculations.

Wyckoff position		#225	#225'	#225"	#216
4*a*	(0, 0, 0)	Ga	Ga	Ni	Mn
4*b*	$\left(\frac{1}{2},\frac{1}{2},\frac{1}{2}\right)$	Mn	Ni	Mn	Ni
8*c* *	$\left(\frac{1}{4},\frac{1}{4},\frac{1}{4}\right)$	Ni	Mn	Ga	Mn
	$\left(\frac{3}{4},\frac{3}{4},\frac{3}{4}\right)$	Ni	Mn	Ga	Ga

* For #216 crystal structure **8*c*** Wyckoff position split into two positions: **4*c***(1/4,1/4,1/4) and **4*d*** (3/4,3/4,3/4).

Table 2. The sign of the magnetic moment of Mn atoms placed at various positions of different crystal structures used in our calculations.

	(0, 0, 0)	$\left(\frac{1}{4},\frac{1}{4},\frac{1}{4}\right)$	$\left(\frac{1}{2},\frac{1}{2},\frac{1}{2}\right)$	$\left(\frac{3}{4},\frac{3}{4},\frac{3}{4}\right)$
FM	>0	>0	>0	>0
FIM-1	>0	>0	<0	<0
FIM-2	<0	>0	>0	>0
FIM-3	<0	>0	>0	>0
FIM-4	>0	>0	<0	>0
FIM-5	>0	>0	>0	<0
FIM-6	>0	>0	<0	<0
FIM-7	<0	>0	<0	>0
FIM-8	<0	>0	>0	<0
FIM-9	<0	>0	<0	<0

3 Results of *ab initio* calculations

Experimental studies of the crystal structure of the investigated alloys shows, that depending on the concentration of excess Mn, Ni, or Ga atoms (above 50%), alloys can crystallize into cubic structures of the symmetry groups #225 and #216 [11]. The research was started with the systematic calculations of the equilibrium energies and magnetic ordering of the mentioned above structures with allowance for different atomic placement. Current research results are shown in Figs. 2-4. In the Fig. 2 the distribution of equilibrium lattice parameter together with regions of stable crystal structure types is shown. These calculations show that only 3 types of crystal structures are realized in the ternary phase diagram. These are #225, #225" (#225 symmetry group with excess Ga in 8*c* Wyckoff positions) and #216. It should be noted that #225' crystal type (#225

symmetry group with excess of Mn atoms in 8*c* Wyckoff positions) is unstable on this diagram.

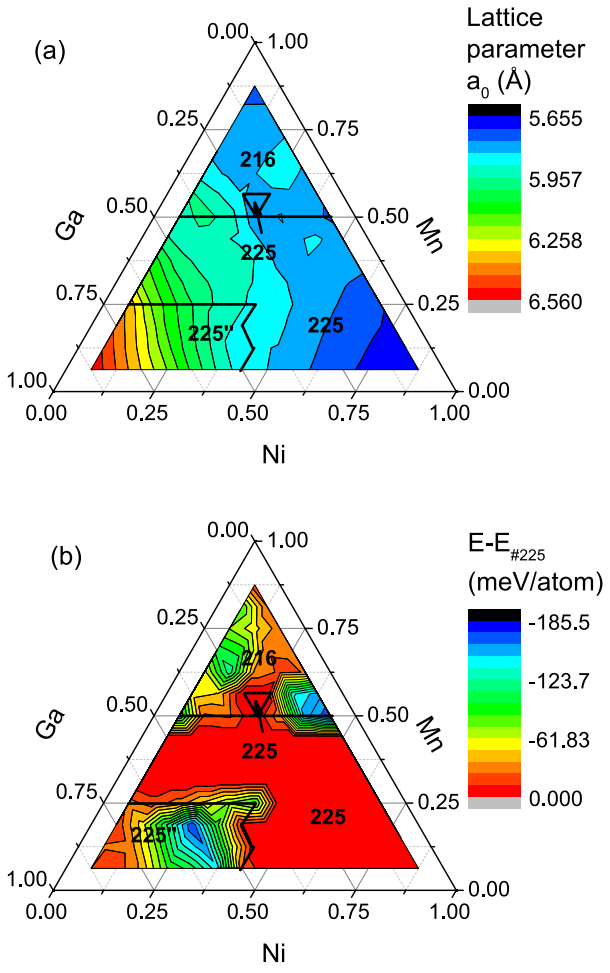

Figure 2. The distribution of (a) the equilibrium lattice parameter and (b) the equilibrium total energy relative to the total energy of #225 crystal lattice mapped on the ternary diagram of Ni-Mn-Ga.

As one can see from Fig. 2(a), the largest lattice parameter (≈ 6.5 Å) is observed at the bottom - left corner of the ternary diagram indicating the compositions with the highest Ga content. Areas with the minimal lattice parameter (≈ 5.7 Å) located at the top and right corners of the diagram corresponding to compositions with highest Mn and Ni concentrations, respectively. The largest lattice parameters for compounds with the excess of Ga is caused by the greater atomic radius of Ga as compared to Mn and Ni whose radii are approximately equal to each other. This result agrees with the previous KKR-CPA calculations [7]. Such agreement shows that, after all, KKR-CPA gives accurate predictions about disordered materials. In the Fig. 2(b) regions of stable crystal structure types together with the distribution of the equilibrium total energy relative to the total energy of #225 crystal lattice together are shown. Calculated energy difference allows us to estimate temperature of phase transitions between phases using the following expression $\Delta E \approx k_B T$ (where k_B is the Boltzman constant).

In Fig. 3(a) we illustrate the mapping of the total magnetic moment on the ternary diagram of Ni-Mn-Ga together with stable magnetic configurations. It can be seen from this distribution, that the largest magnetic moment is observed for alloys with significant Ni excess and with a small content of Ga atoms (≈ 6.5 μ_B). At the same time, areas with the smallest (≈ 0.15 μ_B) values of a magnetization are observed for the compositions with the Mn and Ga atoms excess. Fig. 3(b) shows regions of stable magnetic configurations together with the distribution of the equilibrium total energy relative to the total energy of FM state.

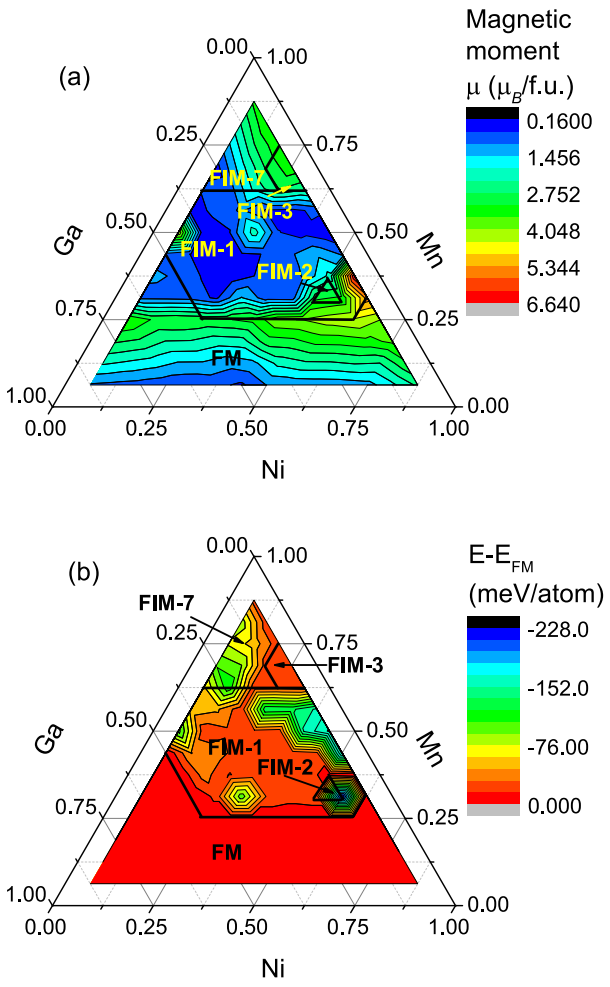

Figure 3. The distribution of (a) the total magnetic moment and (b) the equilibrium total energy relative to the total energy of FM configuration mapped on the ternary diagram of Ni-Mn-Ga.

The calculations also showed that for compositions with Mn excess, FIM ordering type (FIM-3 and FIM-7, see Table 2) is energetically favorable. As for compositions with an excess of Ni and Ga atoms (almost 2/3 of the diagram) an energetically favorable FM ordering except for a small area of compositions with an FIM-1 and FIM-2 ordering. The FIM ordering appears due to AFM interactions between Mn atoms located at the shortest dis-

tance in the cubic lattices of the symmetry groups #225 and #216.

Our calculations show that the most of FIM spin configurations are energetically unfavorable for all the cubic structures of Ni-Mn-Ga.

The formation energies for the cubic lattice of Ni-Mn-Ga alloys mapped on the ternary diagram are shown in Fig. 4.

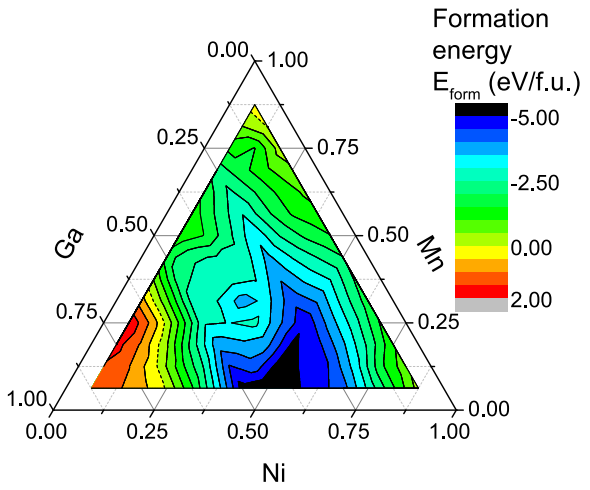

Figure 4. The distribution of the formation energy mapped on the ternary diagram of Ni-Mn-Ga. Dashed lines on diagram correspond to zero formation energy.

It is evident from the figure that the formation energies for the compounds with Ni and Mn excesses atoms have negative values while the positive values of the formation energies indicate that those structures are unstable for alloys with a high Ga content .

4 Conclusions

In this paper the results of investigations of the magnetic and structural properties of Ni-Mn-Ga Heusler alloys with the help of the density functional theory are presented.

Calculations of the ground-state energy of the crystal lattice, the equilibrium lattice parameter, the total magnetic moment, and formation energy were performed for the austenitic (cubic) structure of type $L2_1$ with the help of the VASP *ab initio* code. As an exchange correlation potential, the generalized gradient approximation was considered within the framework of the Perdew-Burke-Ernzerhof potential.

A systematic study of the magnetic and structural properties of Ni-Mn-Ga alloys have been carried out using 16-atoms supercell approach for 105 compositions containing three stoichiometric compositions (Ni_2MnGa, Mn_2NiGa, and Ga_2MnNi) and compositions with the excess of Ni, Mn, and Ga atoms. The calculated equilibrium lattice parameter, total magnetic moment, and formation energy of the cubic phase have been plotted for a ternary diagram of Ni-Mn-Ga alloys. Calculations have shown that a region with Ga atoms excess has the largest lattice parameter and the smallest magnetic moment, whereas regions with an excess of Ni atoms have the smallest lattice parameter. The region with an excess of Mn atoms is also characterized by a small lattice parameter and a small magnetic moment. Crystal formation energy calculations showed that compositions with a significant excess of Ga atoms are unstable in the cubic phase.

Acknowledgments

This work was supported by RSF-Russian Science Foundation No. 17-72-20022/17 (Section 3) and RFBR-Russian Foundation for Basic Research No. 18-32-00507 (Section 2).

References

[1] P. Entel, M.E. Gruner, A. Dannenberg, M. Siewert, S.K. Nayak, H.C. Herper, V.D. Buchelnikov, Mat. Sci. Forum **635**, 3 (2010).

[2] V.D. Buchelnikov, V.V. Sokolovskiy, Phys. Met. Metallogr., **112**, 633 (2011).

[3] V.V. Sokolovskiy, M.A. Zagrebin, V.D. Buchelnikov, Mat. Sci. Foundations, **81**, 38 (2015).

[4] P. Entel, V.D. Buchelnikov, V.V. Khovailo, A.T. Zayak, W.A. Adeagbo, M.E. Gruner, H.C. Herper, E.F. Wassermann, J. Phys. D: Appl. Phys., **39**, 865 (2006).

[5] V. Sokolovskiy, Yu. Sokolovskaya, V.D. Buchelnikov, M. Zagrebin and A.T. Zayak, MATEC Web of Conferences, **33**, 05005 (2015).

[6] V.V. Sokolovskiy, Yu.A. Sokolovskaya, M.A. Zagrebin, V.D. Buchelnikov, A.T. Zayak, Mat. Sci. Forum **845**, 130 (2016).

[7] Yu.A. Sokolovskaya, V.V. Sokolovskiy, M.A. Zagrebin, V.D. Buchelnikov, A.T. Zayak, J. Exp. Theor. Phys. **125**, 104 (2017).

[8] G. Kresse, J. Furthmüller, Phys. Rev. B **54**, 11169 (1996).

[9] G. Kresse, D. Joubert, Phys. Rev. B **59**, 1758 (1999).

[10] J.P. Perdew, K. Burke and M. Enzerhof, Phys. Rev. Lett. **77**, 3865 (1996).

[11] T. Graf, C. Felser, and S.S.P. Parkin, Progr. Sol. St. Chem., **39**, 1 (2011).